Numerical study on the minimum ignition energy of a methane-air mixture

Numerical study on the minimum ignition energy of a methane-air mixture

Haitao Lu[a,b,c], Fuqiang Liu[a,b,*], Kaixing Wang[a,b], Gang Xu[a,b], Henry J. Curran[c]

[a] Institute of Engineering Thermophysics, Chinese Academy of Sciences, Beijing 100190, China;

[b] School of Engineering Science, University of Chinese Academy of Sciences, Beijing 100049, China;

[c] Combustion Chemistry Centre, School of Chemistry, Ryan Institute, National University of Ireland Galway, University Road, Galway, H91 TK33, Ireland.

Abstract

In this paper, a semi-detailed mechanism is used to calculate the minimum ignition energy (MIE) of methane-air mixtures, with all calculations conducted using ANSYS Fluent software. Ignition behaviors between success and failure were analyzed, and the effect of isothermal and adiabatic wall condition, equivalence ratio and electrode wall temperature on the MIE were also numerically investigated. From time histories of temperature and species profiles it is easy to determine when a successful ignition occurs. There are big differences between the MIE predictions using the adiabatic wall and isothermal wall conditions. For different equivalence ratio results, we consider our numerical results to be considerably more accurate than previous studies.

Keywords: Spark ignition, Methane-air mixture, Minimum ignition energy, Numerical analysis

* Corresponding author.
E-mail address: liufuqiang@iet.cn (F. Liu).

1. Introduction

Despite the rapid development of new alternative sources of energy, fossil fuels still play an important role in energy conversion [1]. Methane (CH_4), which is the main component of natural gas, is a relatively clean fossil fuel compared to large hydrocarbons present in conventional gasoline and diesel fuels. Since it can be made by the anaerobic digestion of biomass, methane is regarded as a renewable energy source and is widely used in industry and in our daily lives [2].

Spark ignition is a complex phenomenon involving the coupling of physical and chemical processes. After years of research, the mechanism of ignition is not completely understood. It is known that the formation of the ignition kernel is affected by many factors such as mixture composition, the initial temperature and heat loss to the electrodes. Hill showed that these factors not only change the ignition kernel, but also have an impact on the propagation behavior of a flame [3]. Ballal et al. [4-7] measured the MIE of gaseous and heavy fuels at different equivalence ratios, quenching distances, pressures and turbulence intensities. Cui et al. [8] measured the MIE of methane/air mixtures at elevated temperatures and pressures, and determined that the MIE has a high-order linear relationship with $1/p^2$, but has an approximately linear relationship with $1/T$. However, there are not enough accurate results for many factors including electrode size, electrode gap distance, and spark duration, among others, and sometimes it is not easy to study these experimentally. Therefore, numerical simulation is a good way to capture the transient processes that occur during ignition kernel growth.

Several studies have reported on the growth process of the flame kernel. According to Kravchik et al. [9], kernel growth is divided into two phases; in the first short phase, the pressure wave and the expansion of the plasma kernel control the transformation of mass and energy; in the second phase, diffusion and thermal conduction control mass and energy transfer. Ma et al. [10] established a physical model for the spark ignition of combustible gases, and the MIE of combustible mixtures was predicted by numerical analysis. Sarli et al. [11, 12] performed 3-D large eddy simulations and PIV measurements and found that large-scale vortices play a dominant role in the evolution of the flame structure along the path after ignition. Sarli et al. also found that unsteady flame propagation is very sensitive to the characteristics of the initial flame kernel, in particular its size and turbulence. Turquand d'Auzay et al. [13] simulated the forced ignition of a methane-air mixture at different turbulence intensities using a three-dimensional direct numerical simulation method. Han et al. [14] used simulations to study the effect of different parameters on the MIE including electrode size, electrode gap distance, equivalence ratio, and spark duration. For many numerical studies, natural convection, heat transfer by radiation and ionic species are ignored as they have little effect on kernel growth and flame propagation [15, 16]. Even though many CFD studies have been conducted, many details still need to be calculated, and more accurate computations performed. There are few simulation papers on the effect of heat loss and electrode wall temperature on the MIE of spark ignition. Also, the relative error between simulation and experimental results needs to be further reduced with improved methods and mechanisms.

In this study a methane/air mixture was used to computationally investigate the spark ignition process using a skeletal mechanism reduced from a new chemical kinetic mechanism [17, 18].

64 The ignition behavior of methane, between success and failure is firstly compared. The effects
65 of several factors on MIE are conducted; (i) isothermal wall condition, (ii) adiabatic wall
66 condition, (iii) equivalence ratio and (iv) electrode wall temperature.

67 ## 2. Computational domain and numerical methods

68 ### 2.1 Governing equations

69 In the spark ignition process, chemical and physical processes are very complex at certain
70 times. To characterize the entire process, the following equations are used.

71 (1) The continuity equation:

72 $$\frac{\partial \rho}{\partial t}+\frac{\partial}{\partial x}\left(\rho v_x\right)+\frac{\partial}{\partial r}\left(\rho v_r\right)+\frac{\rho v_r}{r}=0 \tag{1}$$

73 The mass conservation equation is shown in Eq. (1). In Eq. (1), ρ is the density, x is the axial
74 coordinate, r is the radial coordinate, v_x is the axial velocity, and v_r is the radial velocity.

75 (2) Momentum conservation equations

76 $$\begin{aligned}&\frac{\partial}{\partial t}\left(\rho v_x\right)+\frac{1}{r}\frac{\partial}{\partial x}\left(r\rho v_x v_x\right)+\frac{1}{r}\frac{\partial}{\partial r}\left(r\rho v_r v_x\right)=-\frac{\partial p}{\partial x}+\frac{1}{r}\frac{\partial}{\partial x}\left[r\mu\left(2\frac{\partial v_x}{\partial x}-\frac{2}{3}(\nabla\cdot\vec{v})\right)\right]\\&+\frac{1}{r}\frac{\partial}{\partial r}\left[r\mu\left(\frac{\partial v_x}{\partial r}+\frac{\partial v_r}{\partial x}\right)\right]\end{aligned} \tag{2}$$

77 $$\begin{aligned}&\frac{\partial}{\partial t}\left(\rho v_r\right)+\frac{1}{r}\frac{\partial}{\partial x}\left(r\rho v_x v_r\right)+\frac{1}{r}\frac{\partial}{\partial r}\left(r\rho v_r v_r\right)=-\frac{\partial p}{\partial r}+\frac{1}{r}\frac{\partial}{\partial x}\left[r\mu\left(\frac{\partial v_r}{\partial r}+\frac{\partial v_x}{\partial r}\right)\right]\\&+\frac{1}{r}\frac{\partial}{\partial r}\left[r\mu\left(2\frac{\partial v_r}{\partial r}-\frac{2}{3}(\nabla\cdot\vec{v})\right)\right]-2\mu\frac{v_r}{r^2}\frac{2\mu}{3r}(\nabla\cdot\vec{v})+\rho\frac{v_z^2}{r}\end{aligned} \tag{3}$$

78 Where

$$\nabla \cdot \vec{v} = \frac{\partial v_x}{\partial x} + \frac{\partial v_r}{\partial r} + \frac{v_r}{r} \tag{4}$$

Eqs. (2) and (3) are the axial and radial momentum conservation equations, where μ is the molecular viscosity and p is the pressure.

(3) Energy conservation equation

$$\frac{\partial}{\partial t}(\rho E) + \nabla \cdot (\vec{v}(\rho E + p)) = -\nabla \cdot \left(\sum_j h_j J_j \right) + S_h \tag{5}$$

(4) Species mass conservation equation

$$\frac{\partial}{\partial t}\left(\rho Y_i\right) + \nabla \cdot \left(\rho \vec{v} Y_i\right) = -\nabla \cdot \vec{J}_i + R_i + S_i \tag{6}$$

$$\vec{J}_i = -\rho D_{i,m} \nabla Y_i - D_{T,i} \frac{\nabla T}{T} \tag{7}$$

Eqs. (5) and (6) are the energy and species mass conservation equations, respectively, where E is the internal energy, S_h is the energy source from heating, Y_i is the local mass fraction of each species i, where R_i is the net rate of production of species i by chemical reaction and S_i is the rate of creation by addition from the dispersed phase plus any user-defined sources. $\vec{J}_i$ is the diffusion flux of species i. In Eq. (7), $D_{i,m}$ is the mass diffusion coefficient for species i in the mixture, and $D_{T,i}$ is the thermal (Soret) diffusion coefficient.

2.2 Assumptions for simplicity of computations

To accelerate simulation work and reduce the number of calculation, some assumptions were made according to the following four assumptions from the work of Han et al. [14].

(1) The mixture gases are considered as ideal gases

(2) The Soret, Dufour, and pressure effects are negligible

(3) The influence of the magnetic and electrical fields can be ignored

(4) Heat transfer by radiation, ionic and electronic species is neglected

2.3 Initial and boundary conditions

In this paper, there is no flow before ignition, and the spark in the quiescent combustible mixture is supposed to be cylindrical. If a 3-D simulation were conducted, the differences in the results in the circumferential direction would be negligible. For the 2-D axisymmetric simulations, accurate axial and radial results can be obtained using a reduced number of meshes and with a much shorter computational time. According to Han et al. the initial shape of the flame in gas mixtures is axisymmetric, and the 2-D axisymmetric model in ANSYS Fluent software was used [19]. As shown in Fig. 1, the computational region is 5 × 5 mm in green, the electrode radius R = 0.3 mm, the spark channel radius R_C = R = 0.3 mm, and the electrode gap distance L = 1.0 mm. According to Sloane et al. [20], when R_C is smaller than 0.3 mm, the MIE is almost constant, and so 0.3 mm was chosen for R_C.

The initial gas was a CH_4/air mixture, at an initial temperature of 300 K and at a pressure of 1 atm. For most cases the initial gases were stoichiometric mixtures, and the compositions were changed when equivalence ratios were studied. There were no surface reactions on the electrode boundary, the no-slip condition was used, and all gradients of the species on the surface were set to zero. The temperature of the electrode was changed according to different computational conditions.

In this paper, a certain constant ignition energy density q was used to simulate the constant value of the electric power during the ignition process. The ignition energy, Q, was calculated using $Q = q \times \tau_i \times V$, where q is ignition energy density, τ_i is the spark duration and V is the volume of the spark channel. 50 μs was chosen for τ_i for most cases, since an optimum value of the MIE can be obtained for spark durations in the range 3 – 100 μs [21]. The z-axis was considered to axisymmetric, the r-axis was considered as the line of symmetry and other two boundaries were treated as outlets.

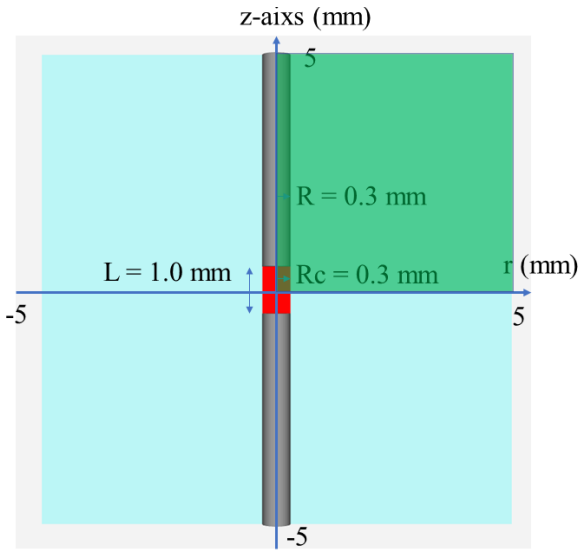

Fig. 1. Scheme of computational domain.

2.4 Numerical method

A semi-detailed mechanism containing 39 species and 231 reactions was used[18]. The specific heat, thermal conductivity, viscosity and mass diffusivity were calculated using the CHEMKIN-CFD Solver [19], and mixture averaged mass diffusivities for each species were used in the mass diffusivity calculation.

In this paper, the ANSYS Fluent software [19] was used, and finite-rate model was conducted

by CHEMKIN-CFD solver in Fluent. For the finite-rate kinetic model, general reaction-rate expressions are used to calculate the chemical source terms. The net source of a chemical species i due to reaction is computed as the sum of the reaction sources over the N_R reactions that the species participate in:

$$R_i = M_{w,i} \sum_{r=1}^{N_R} \hat{R}_{i,r} \tag{8}$$

where $M_{w,i}$ is the molecular weight of species i and $\hat{R}_{i,r}$ is the molar rate of reaction/destruction of species i in reaction r. For more details about finite-rate modeling can be found in the work by Sloane and Rooney [10].

The grid size was set at 0.05 mm and the time step to 1 μs according to Han et al. [14, 22]. The coupled method was used to adjust the velocity and pressure fields, and a second-order upwind scheme was employed for convective terms [23].

3. Results and discussion

3.1 Ignition behavior between success and failure

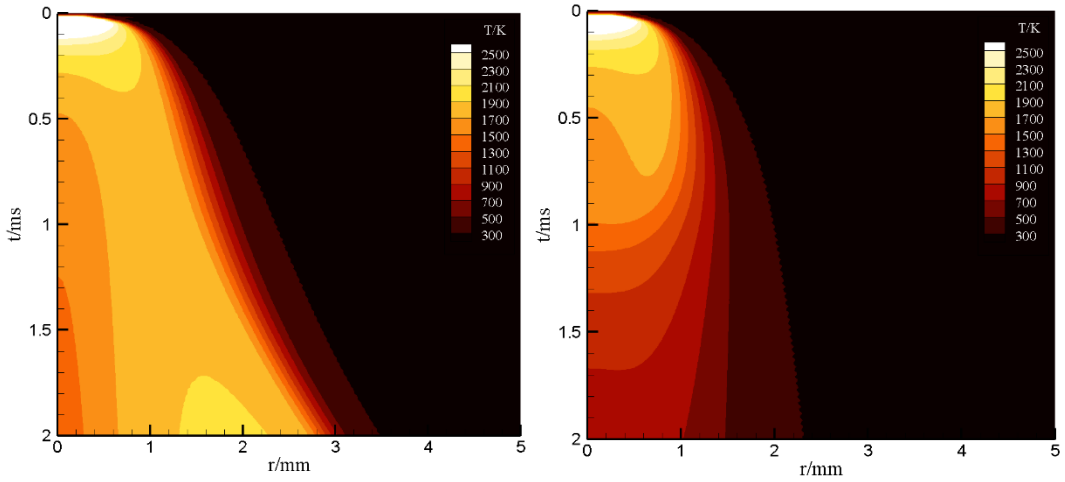

(a) q = 60 GW/m^3 (b) q = 45 GW/m^3

Fig. 2. Time history of temperature at z = 0 mm section.

When computing the MIE, the definition of ignition success is very significant. Successful ignition is defined as the time when a flame kernel is formed at a certain place and it can propagate steadily [14]. Based on the temperature time history at the z = 0 mm section, the state of ignition can be judged. On the basis of Fig. 2(a), the high temperature area can expand to the ambient cold region with time using q = 60 GW/m^3 (Q = 0.848 mJ*);* Meanwhile Fig. 2(b), using q = 45 GW/m^3 (Q = 0.636 mJ*),* shows that it cannot extend and it even shrinks with time (τ), and moreover the maximum temperature decreases. In this way, the MIE can be simulated in different cases.

Maximum temperature histories are shown in Fig. 3. As we can see, the temperature increases quickly with the start of ignition, and after τ = 50 μs, it decreases sharply to 2000 K. At τ = 2 ms, the maximum temperature using q = 45 GW/m^3 is lower than 1000 K, which means the flame has quenched; while the maximum temperature using q = 60 GW/m^3 remains steady at 2000 K.

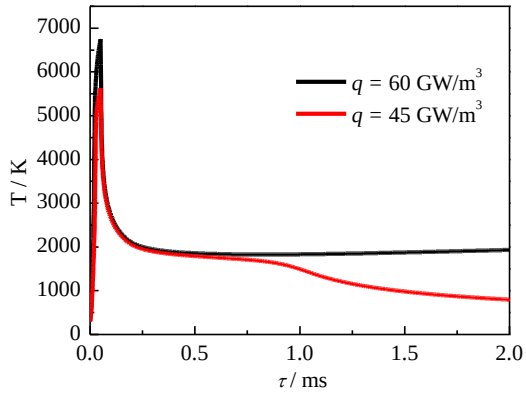

Fig. 3. Maximum temperature history for q = 60 GW/m^3 and q = 45 GW/m^3.

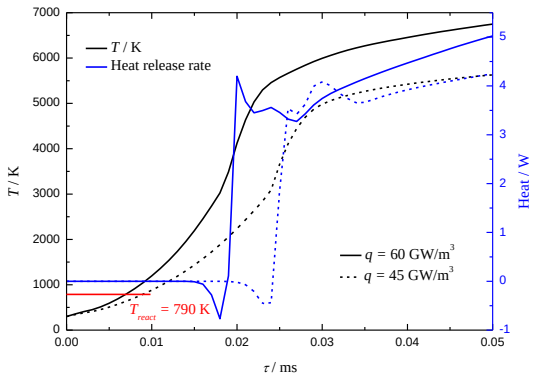

Fig. 4. Maximum temperature and heat release ratio histories during the first 50 μs.

Figure 4 shows the maximum temperature and heat release ratio histories during first 50 μs. The red line shows the temperature (T = 790 K) at which reaction begins. In the initial phase, reaction begins with the reaction $CH_4 + O_2 = \dot{C}H_3 + H\dot{O}_2$, after which, $\dot{C}H_3$ radicals react with O_2 to produce $CH_3\dot{O}_2$ radicals $\dot{C}H_3 + O_2 = CH_3\dot{O}_2$. At low temperatures the reaction $CH_3\dot{O}_2 + \dot{C}H_3 = CH_3\dot{O} + CH_3\dot{O}$ is important in promoting reactivity. The temperature gradually increases due to a constant energy input, before τ = 18 μs for q = 60 GW/m^3 (τ = 24 μs for q = 45 GW/m^3) most reactions are endothermic, and the mixture burns at τ = 20 μs (τ = 26 us for q = 45 GW/m^3) with a sharp increase of heat release ratio. After a few microseconds, a flame front is formed, and propagates steadily towards the unburned mixture region.

Figure 5 shows the profiles of some major species in radial direction at different times. At τ = 40 μs the temperature is high due to heat release. At high temperatures (≥ 2000 K), it is easy to produce radical species such as $\dot{O}$, $\dot{O}H$ and $\dot{C}H_3$ in the spark channel. Since there is a difference in energy density, the mass fraction of radical species in the solid lines are higher than the short dashed lines at r = 0 – 0.5 mm. Figure 5(a) shows that the spark kernel of the high energy density ignition can propagate quickly. At τ = 1500 μs the maximum temperature of q = 60 GW/m^3 is approximately 2000 K, and the flame front propagates to r = 2.2 mm.

From the temperature time history and the profiles of the major species, there are significant differences between successful and failed ignition events, so the state of ignition can be clearly

defined.

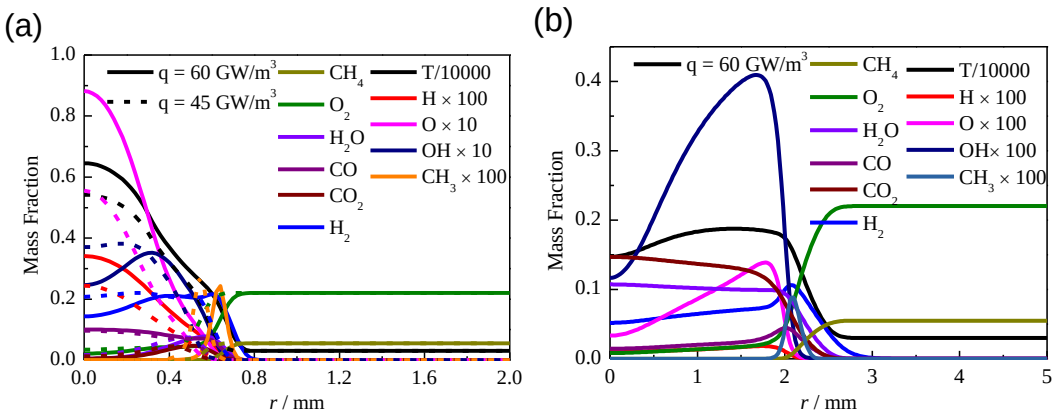

Fig. 5. Profiles of some major species at (a) τ = 40 μs and (b) τ = 1500 μs.

3.2 Ignition behavior between isothermal and adiabatic wall condition

In order to study heat loss during the ignition process, two simulations, Case 1 and Case 2 were performed, with details of the conditions given in Table 1.

Table 1. Case conditions

Name	Wall condition	MIE / mJ
Case 1	Isothermal, T = 300 K	0.707
Case 2	Adiabatic	0.254

Figure 6 shows the time histories for these two cases. The flame kernel for Case 1 spreads quickly initially, and at τ = 50 μs, the high temperature region expanded at approximately r = 1 mm; while the boundary position of the adiabatic flame kernel was approximately r = 0.4 mm. Adiabatic ignition can propagate stably after τ = 50 μs and the temperature of burned region is higher than for isothermal ignition. Figure 7 shows the maximum temperature history and it reflects the different character of these two wall-condition ignitions. Case 1 attains a higher

temperature than Case 2 initially, but the temperature in Case 1 falls sharply after the energy supply is stopped.

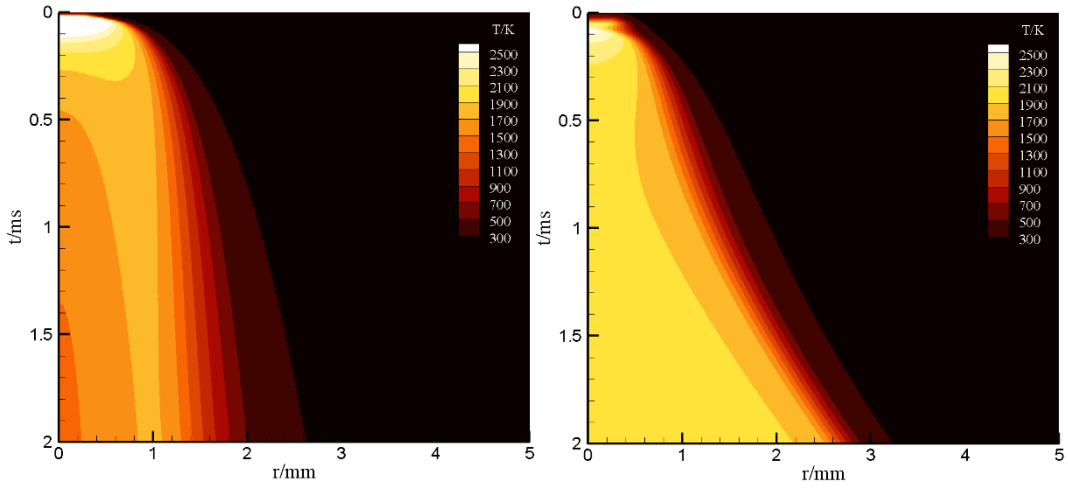

Fig. 6. Temperature/time histor at the z = 0 mm section. (a) Case 1: isothermal wall condition and (b) Case 2: adiabatic wall condition.

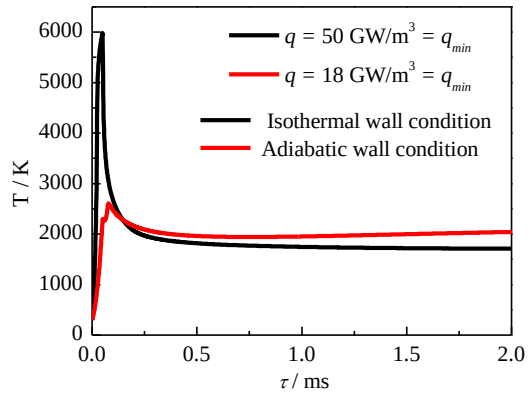

Fig. 7. Maximum temperature histories for two cases.

Temperature and velocity contours are shown in Fig. 8 and Fig. 9. Initially the energy density of Case 1 is q_{min} = 50 GW/m^3 which is higher than for Case 2 where q_{min} = 18 GW/m^3. The high temperature region of Case 1 extends out at high velocity. Due to heat loss from the electrode surface, the fall in temperature in Case 1 was big, and the flame propagation velocity

becomes slow. For Case 2, after successful ignition, the flame burned steadily.

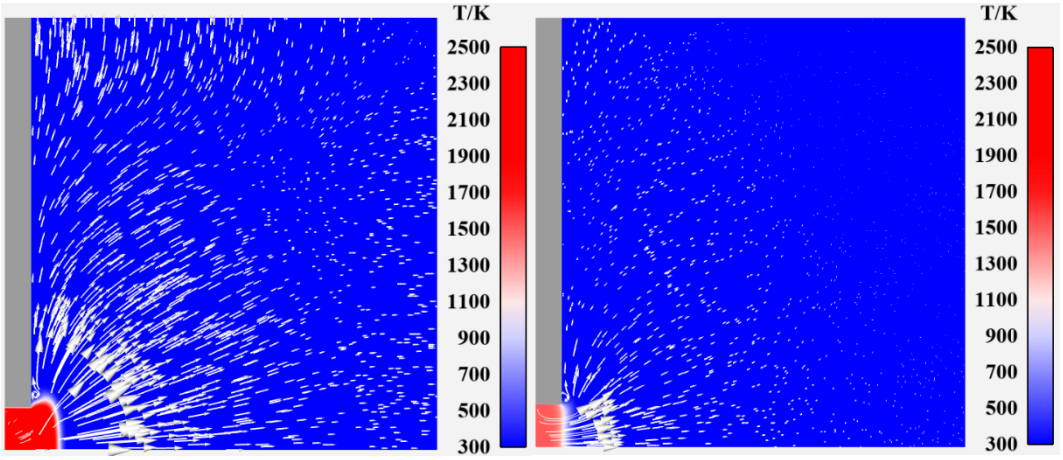

(a) (b)

Fig. 8. Temperature and velocity contour at τ = 40 μs. (a) Case 1: isothermal wall condition and (b) Case 2: adiabatic wall condition.

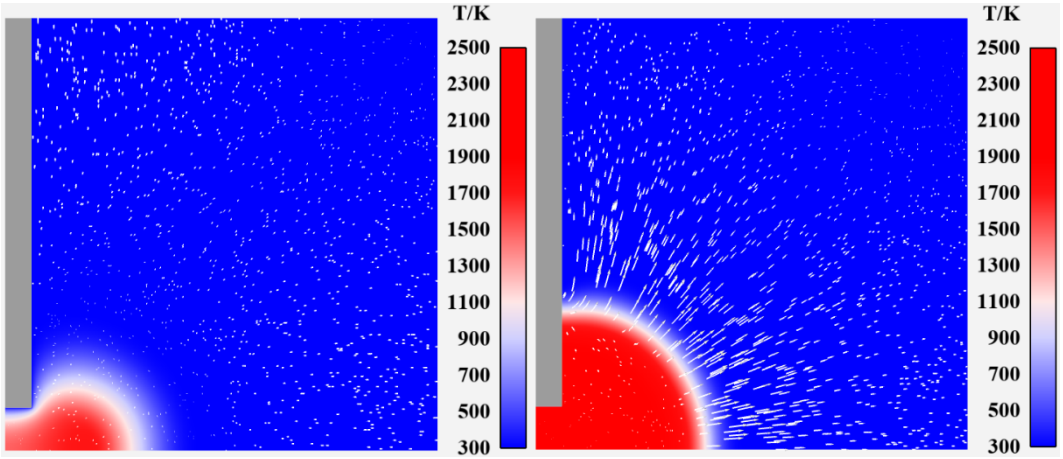

(a) (b)

Fig. 9. Temperature and velocity contour at at τ = 1500 μs. (a) Case 1: isothermal wall condition and (b) Case 2: adiabatic wall condition.

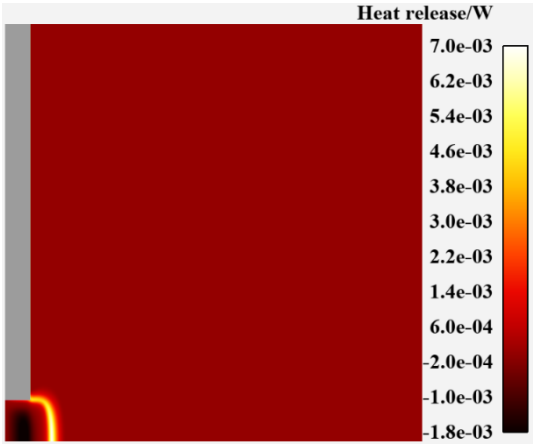

Fig. 10. Heat release contour at τ = 40 μs in Case 1: isothermal wall condition.

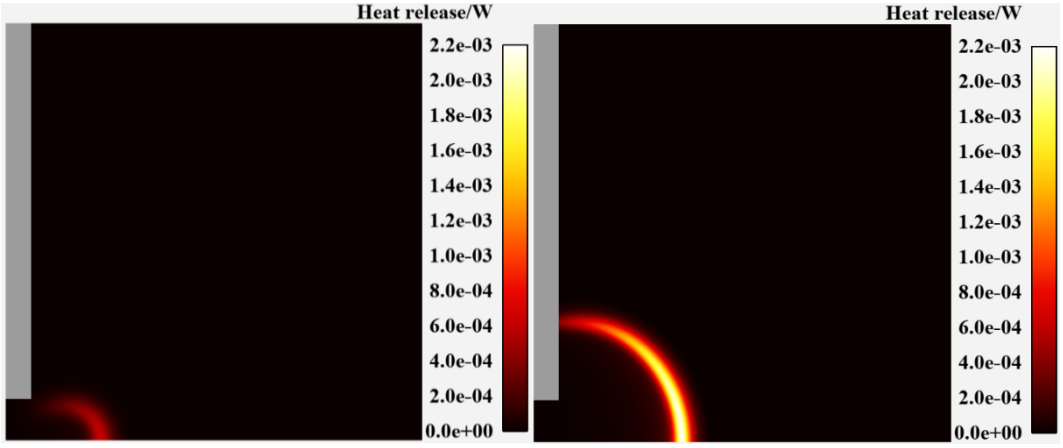

(a) (b)

Fig. 11. Heat release contour at τ = 1500 μs. (a) Case 1: isothermal wall condition and (b) Case 2: adiabatic wall condition.

Figures 10 and Figure 11 show heat release contours at τ = 40 μs and τ = 1500 μs. At τ = 40 μs, for Case 1 there is a strong heat release, while there is no heat release for Case 2 since the temperature between the electrodes is low. At the propagation phase the heat release become weak for Case 1, while the heat release of Case 2 is very strong.

Comparing the MIE for Cases 1 and 2, more energy is consumed for the isothermal wall condition, and the MIE of Case 2 is 35.93% that of Case 1, Fig. 12. Moreover, 64.07% of the

energy consumed is used to heat both the mixture and the electrode wall.

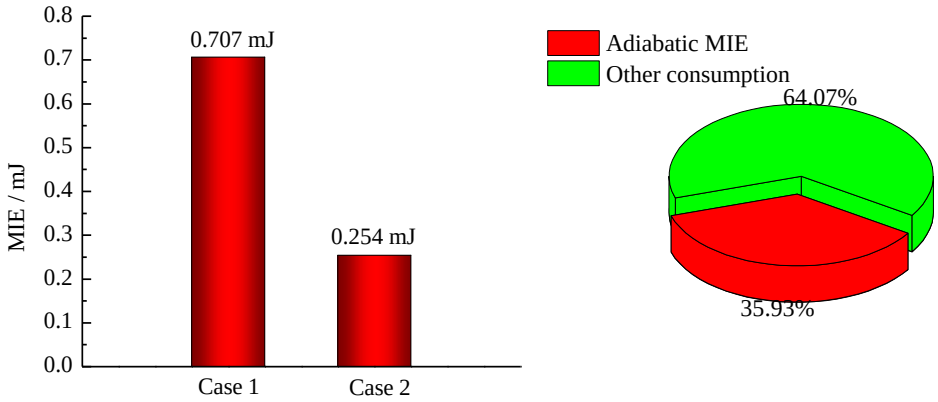

(a) MIE of two cases (b) Distribution of Energy

Fig. 12. MIE comparison of two cases.

The heat loss and the release rate of both cases are shown in Fig. 13. For the isothermal wall condition the heat release rate and the heat loss rate remain low in the first 3 ms, while it increases rapidly after 1ms for the adiabatic wall condition. The total energy, including heat production and energy input, of the isothermal wall condition ignition is 0.925 mJ over 50 μs, and heat loss is 0.171 mJ. 18.46% of the energy is lost to the wall, with the remaining 81.54% of the energy used to heat and ignite the mixture. Therefore, when designing a spark igniter, an electrode wall composed of a lower thermal conductivity material is more effective in decreasing the MIE and improving ignition performance.

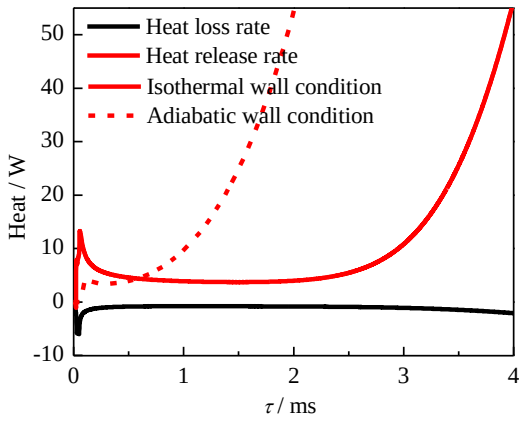

Fig. 13. Heat loss rate and heat release rate of two cases.

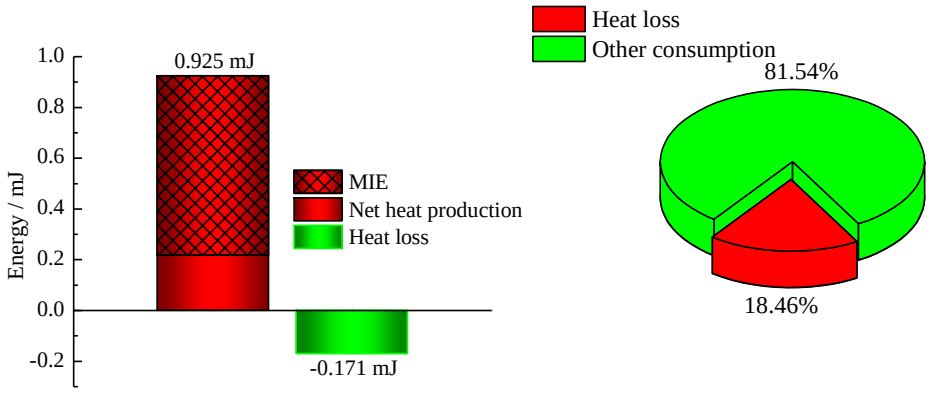

(a) Energy production and loss in 50 μs (b) Energy distribution in 50 μs

Fig. 14. Energy distribution of isothermal wall condition ignition.

3.3 Effect of the equivalence ratio on the MIE

Simulations of the effect of equivalence ratio on the MIE were conducted, and these results were compared with Han's computations and Lewis' experimental work [14, 24]. For φ = 0.7, 100 μs was chosen for τ_i to ensure a converged solution, so some numerical problems with high energy density addition for τ_i = 50 μs could be avoided. The simulation results in Fig. 15 show a very good trend compared to the experiment data; the minimum MIE of different equivalence ratios was close to 1.0 in the fuel-lean mixture region. Compared to Han's computation, the simulations in this paper are more accurate. In Han's paper, a simplified transport model was used. The effective thermal conductivity, λ, was calculated from C_p and T using a polynomial fit, and the effective diffusivity of species i was calculated using the Lewis number. In this paper, for material properties such as specific heat, viscosity, thermal conductivity, mass diffusivity and thermal diffusion, they are computed using the CHEMKIN-CFD solver and the mechanism files. Mixture averaged mass diffusivities for each species were used in the calculations. Results are improved using this methodology.

Figure 16 shows heat loss ratios of different equivalence ratios. In Fig. 16,

$$Ratio\,1 = \frac{q_{Heat\ loss}}{MIE + q_{Heat\ release}} \tag{7}$$

$$Ratio\,2 = \frac{q_{Heat\ loss}}{MIE} \tag{8}$$

For both Ratio 1 and Ratio 2, minimum values are obtained at φ = 0.9, with average values of Ratio 1 being about 20% and average values of Ratio 2 are 5% higher than for Ratio 1. Figure 16 indicated that a lower MIE will lose less energy to the electrode wall.

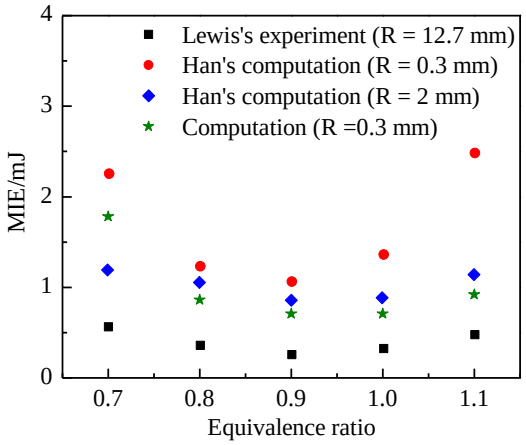

Fig. 15. Effect of the equivalence ratio on the MIE.

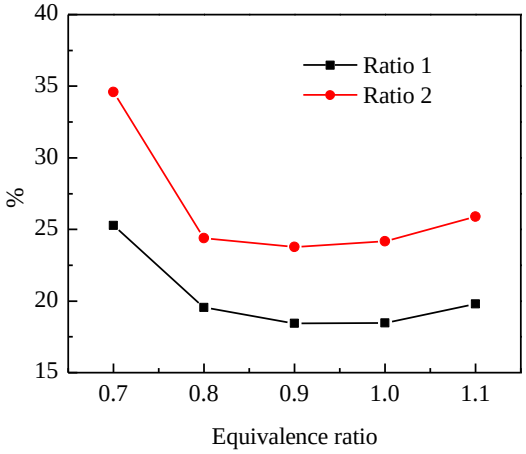

Fig. 16. Heat loss ratios during ignition period.

3.4 Effect of the electrode wall temperature on the MIE

Figure 16 shows that 25% of the MIE is consumed by heat loss to the wall, so wall temperature effects on the MIE were studied. The effect of wall temperature on the MIE is shown in Fig. 17, and it is observed that as the temperature increases, the MIE decreases. Figure 18 shows the heat loss rate to the wall at wall temperatures of T = 450 K and T = 600 K are higher than for the mixture at temperature of 300 K, because initially heat transfers from the wall to the mixture. When the mixture temperature becomes higher than the wall, energy is transferred back to the wall. At higher wall temperatures, a lower MIE is needed. Moreover, on heating the electrode wall, ignition becomes easier. Due to the contribution of the electrode wall temperature, ignition under extreme conditions, such as high altitude relight and plateau ignition, can be achieved. So it is much better for a designer to add a heating system on the electrode wall of the spark igniter to decrease the MIE of the mixture and enhance ignition performance.

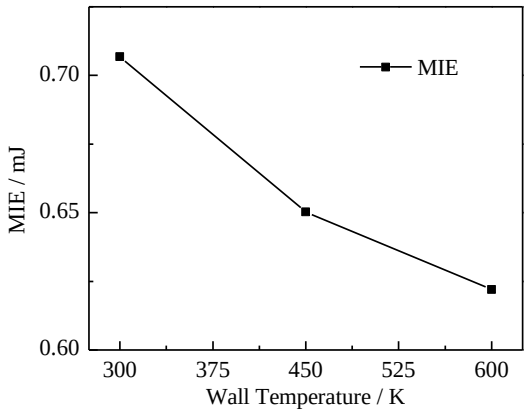

Fig. 17. Effect of the wall temperature on the MIE.

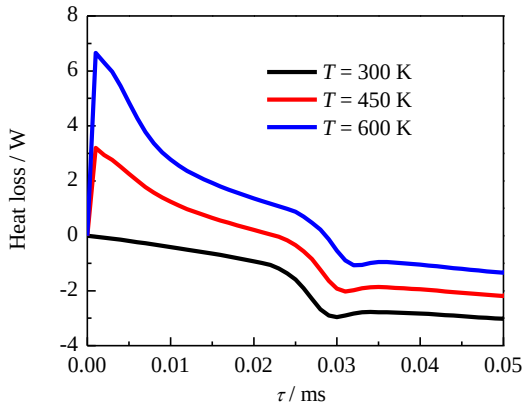

Fig. 18. Heat loss to the wall at different wall temperatures.

4. Conclusions

Ignition behaviors between success and failure were numerically investigated for isothermal and adiabatic wall conditions, at different equivalence ratios and electrode wall temperatures to determine the effect on the MIE for methane/air mixtures. From our computational results, the following conclusions were reached.

(1) Successful ignition can be determined from the temperature/time history at the z = 0 mm section. Maximum temperature histories and species profiles were determined with significant differences being observed between successful ignitions and failures.

(2) For the adiabatic wall condition, ignition costs much less energy than for the isothermal wall condition. A sharp change in the temperature history was observed for the isothermal wall condition ignition while in the adiabatic condition it was very flat. For the stoichiometric methane/air mixture at 1 atm, 18.46% of the energy was taken up by heat loss to the wall, and the remaining 81.54% was used to heat and ignite mixture. Thus, an electrode wall with a lower thermal conductivity material is very helpful in decreasing the MIE required and improving the ignition performance of a spark igniter.

(3) At different equivalence ratios, the minimum MIE is close to 0.9, and numerical results with the CHEMKIN-CFD solver and the latest skeletal mechanism are in good agreement with the experiment data and they are better than previous simulation works. A lower MIE will lose less energy to the electrode wall.

(4) For higher wall temperatures, a lower MIE is needed. And after heating the electrode, it is much easier to ignite a mixture. When a heating system is added to the electrode wall of the spark igniter, the MIE of the mixture is smaller and the ignition performance is enhanced.

The MIE of a methane-air mixture was studied using CFD in this paper. Some methods such as choosing a lower thermal conductivity material and adding a heating system to the electrode wall are proposed to improve ignition performance. However, there are still some factors that affect the MIE such as the ways the energy is discharged, the turbulence intensity and initial conditions of temperature and pressure that should be studied in flow and real engine conditions.

Acknowledgements

The authors would like to acknowledge the National Science and Technology Major Project (2017-III-0007-0032). Haitao Lu acknowledges financial support from China Scholarship Council.

References

[1] Agency IE. World Energy Outlook 2019. 2019.

[2] Molino A, Nanna F, Migliori M, Iovane P, Ding Y, Bikson B. Experimental and simulation results for biomethane production using peek hollow fiber membrane. Fuel 2013;112:489-93.

[3] Hill PG. Cyclic variations and turbulence structure in spark-ignition engines. Combustion and Flame 1988;72(1):73-89.
[4] Ballal DR, Lefebvre AH. The influence of flow parameters on minimum ignition energy and quenching distance. Symposium (International) on Combustion 1975;15(1):1473-81.
[5] Ballal DR, Lefebvre AH. IGNITION AND FLAME QUENCHING IN FLOWING GASEOUS MIXTURES. Proc R Soc London Ser A 1977;357(1689):163-81.
[6] Ballal DR, Lefebvre AH, Gaydon AG. Ignition and flame quenching of quiescent fuel mists. Proceedings of the Royal Society of London A Mathematical and Physical Sciences 1978;364(1717):277-94.
[7] Ballal DR, Lefebvre AH. A general model of spark ignition for gaseous and liquid fuel-air mixtures. Symposium (International) on Combustion 1981;18(1):1737-46.
[8] Cui G, Zeng W, Li Z, Fu Y, Li H, Chen J. Experimental study of minimum ignition energy of methane/air mixtures at elevated temperatures and pressures. Fuel 2016;175:257-63.
[9] Kravchik T, Sher E. Numerical modeling of spark ignition and flame initiation in a quiescent methane-air mixture. Combustion and Flame 1994;99(3):635-43.
[10] Ma Q, Zhang Q, Pang L. Theoretical model of minimum ignition energy prediction for methane-air mixture. Gaoya Wuli Xuebao/Chinese Journal of High Pressure Physics 2012;26:301-5.
[11] Di Sarli V, Di Benedetto A, Russo G, Jarvis S, Long E, Hargrave G. Large Eddy Simulation and PIV Measurements of Unsteady Premixed Flames Accelerated by Obstacles. Flow, Turbulence and Combustion 2009;83:227-50.
[12] Di Sarli V, Di Benedetto A, Russo G. Sub-grid scale combustion models for large eddy simulation of unsteady premixed flame propagation around obstacles. Journal of Hazardous Materials 2010;180(1-3):71-8.
[13] Turquand d'Auzay C, Papapostolou V, Ahmed SF, Chakraborty N. On the minimum ignition energy and its transition in the localised forced ignition of turbulent homogeneous mixtures. Combustion and Flame 2019;201:104-17.
[14] Han J, Yamashita H, Hayashi N. Numerical study on the spark ignition characteristics of a methane–air mixture using detailed chemical kinetics: Effect of equivalence ratio, electrode gap distance, and electrode radius on MIE, quenching distance, and ignition delay. Combustion and Flame 2010;157(7):1414-21.
[15] Thiele M, Selle S, Riedel U, Warnatz J, Schießl R, Maas U. A Detailed Two-Dimensional Numerical Study of Spark Ignition Including Ionization. SAE Transactions 2002;111:1820-5.
[16] Foucher F, Burnel S, Mounaïm-Rousselle C. Evaluation of burning rates in the vicinity of the piston in a spark-ignition engine. Proceedings of the Combustion Institute 2002;29(1):751-7.
[17] Burke U, Somers KP, O'Toole P, Zinner CM, Marquet N, Bourque G, et al. An ignition delay and kinetic modeling study of methane, dimethyl ether, and their mixtures at high pressures. Combustion and Flame 2015;162(2):315-30.
[18] Lu H, Liu F, Wang Y, Fan X, Yang J, Liu C, et al. Mechanism reduction and bunsen burner flame verification of methane. Energies 2019;12(1).

[19] ANSYS. ANSYS Fluent Theory Guide. Release 19.0 ed. San Diego, CA, USA: ANSYS Inc.; 2018.
[20] Sloane TM, Ronney PD. A Comparison of Ignition Phenomena Modelled with Detailed and Simplified Kinetics. Combustion Science and Technology 1993;88(1-2):1-13.
[21] Frendi A, Sibulkin M. Dependence of Minimum Ignition Energy on Ignition Parameters. Combustion Science and Technology 1990;73(1-3):395-413.
[22] Han J, Yamashita H, Hayashi N. Numerical study on the spark ignition characteristics of hydrogen–air mixture using detailed chemical kinetics. International Journal of Hydrogen Energy 2011;36(15):9286-97.
[23] Barth T, Jespersen D. The design and application of upwind schemes on unstructured meshes. 27th Aerospace Sciences Meeting. American Institute of Aeronautics and Astronautics; 1989.
[24] Lewis B, Von Elbe G. Combustion, Flames and Explosions of Gases (Third Edition). San Diego: Academic Press; 1987.